Mon. Not. R. Astron. Soc. **450**, 4016–4024 (2015) Printed 28 August 2015 (MN LATEX style file v2.2)

Magnetized stars with differential rotation and a differential toroidal field

Kotaro Fujisawa ⋆
Advanced Research Institute for Science and Engineering, Waseda University, 3-4-1 Okubo, Shinjuku-ku, Tokyo 169-8555, Japan

Accepted 2015 April 21. Received 2015 April 13; in original form 2015 February 25

ABSTRACT
We have succeeded in obtaining magnetized equilibrium states with differential rotation and *differential* toroidal magnetic fields. If an internal toroidal field of a protoneutron star is wound up from the initial poloidal magnetic field by differential rotation, the distribution of the toroidal magnetic field is determined by the profile of this differential rotation. However, the distributions of the toroidal fields in all previous magnetized equilibrium studies do not represent the magnetic winding by the differential rotation of the star. In this paper, we investigate a formulation of a *differential* toroidal magnetic field that represents the magnetic field wound up by differential rotation. We have developed two functional forms of *differential* toroidal fields which correspond to a v-constant and a j-constant field in analogy to differential rotations. As the degree of the *differential* becomes very high, the toroidal magnetic field becomes highly localized and concentrated near the rotational axis. Such a *differential* toroidal magnetic field would suppress the low-$T/|W|$ instability more efficiently even if the total magnetic field energy is much smaller than that of a non-*differential* toroidal magnetic field.

Key words: stars: magnetic field – stars: neutron – stars: rotation

1 INTRODUCTION

A rapidly rotating protoneutron star are produced by a core collapse supernova, accretion-induced collapse white dwarf. They can be subject to well-known non-axisymmetric instabilities (Andersson 2003). Stellar deformations caused by rotation and the non-axisymmetric instabilities can generate strong gravitational wave signals, with the global $m = 2$ instabilities particularly related to gravitational wave production. Thus, a rapidly rotating protoneutron star is a good source of gravitational radiation.

The development of non-axisymmetric instabilities is characterized by the energy ratio $\beta = T/|W|$, where T is the rotational energy and W is the gravitational potential energy of the rotating star. Studies of these instabilities were obtained in the nineteenth century (e.g., Bryan 1889). Uniformly rotating incompressible fluids exhibit the $m = 2$ f-mode dynamical instability when the value of β satisfies the threshold $\beta > 0.27$ (see also Chandrasekhar 1969). On the other hand, there exists a secular instability which is driven by dissipative processes, such as viscosity and gravitational radiation, which grows when the value of β is larger than 0.14 (see also numerical calculations by Shibata & Karino 2004). This threshold is easier to satisfy than the threshold for dynamical bar-mode instability, but the growth time-scale is much longer because the typical time-scale of the dissipation process is much larger than that of a dynamical time-scale (Lai & Shapiro 1995).

The instability situation changes if we introduce sufficiently large differential rotation. The linear analysis of a rapidly rotating star by Karino & Eriguchi (2003) showed that the threshold of the dynamical instability decreases when the degree of the differential rotation is sufficiently large. Many numerical simulations have confirmed that $m = 1$ or $m = 2$ non-axisymmetric instabilities can appear at a much lower β than 0.27 if a sufficiently large differential rotation is present (for example, $\beta \sim 0.14$ in Centrella et al. 2001). This non-axisymmetric instability is referred to as low-$T/|W|$ instability, and it can occur even for $\beta \sim 0.01$ (Shibata et al. 2002, 2003; Saijo et al. 2003). Although numerical simulations have shown their existence, the physical origin of low-$T/|W|$ instabilities remains unclear. The instabilities are associated with the presence of a corotation resonance point inside the star (Watts et al. 2005; Saijo & Yoshida 2006). The wave pattern speed of an unstable mode equals the local background fluid rotational velocity at the point. Corotation resonance has long been known to be a key factor for instabilities in various astrophysical contexts, such as the corotational instabilities for thin accretion discs, the spiral pattern in galaxies (Shu 1992), and the Papaloizou-Pringle instability for accretion tori (Papaloizou & Pringle 1984; Fu & Lai 2011a). By performing time evolutions of linear perturbations of differential rotating stars, Passamonti & Andersson (2015) recently found that the $\ell = m = 2$ f-mode becomes unstable as soon as a corotation point develops inside the star. The low-$T/|W|$ instabilities are thus a subclass of local shear instabilities.

The effect of magnetic fields is a significant issue concerning

⋆ E-mail: fujisawa@heap.phys.waseda.ac.jp

these instabilities. Many numerical simulations have shown that low-$T/|W|$ instability may develop in some proto-neutron stars with rapid rotation during stellar core-collapses (Ott et al. 2005, 2007; Shibata & Sekiguchi 2005) because of their sufficiently large differential rotations. On the other hand, recent magnetohydrodynamical simulations have shown that the dynamical bar-mode instability can be suppressed by magnetic force (Camarda et al. 2009; Franci et al. 2013). Since large toroidal fields can be wound up from an initial poloidal magnetic field by differential rotation and amplified by magneto-rotational-instabilities (Akiyama et al. 2003; Shibata et al. 2006; Obergaulinger et al. 2006; Obergaulinger et al. 2009; Masada et al. 2012; Sawai et al. 2013), rapidly rotating proto-neutron stars are expected to have large toroidal magnetic fields, which would suppress the low-$T/|W|$ instability.

Contrasting with the many numerical simulation studies, Fu & Lai (2011b) investigated the effect of a purely toroidal magnetic field on the low-$T/|W|$ instability by applying linear analysis to a cylindrical star with a simple model of the toroidal magnetic field (Ostriker 1965; Saijo & Yoshida 2006). They found that the toroidal magnetic field suppresses the low-$T/|W|$ instability when the total toroidal magnetic energy $\mathcal{M}$ is in the order of 0.2 T or larger. Such magnetic energy corresponds to toroidal fields of a few 10^{16} G in their magnetic field model. This study also found that the corotation point is split into two slow magnetosonic resonances in the presence of strong toroidal fields. Therefore, the unstable mode in the presence of the toroidal field is determined by both corotation and slow magnetosonic resonances inside the magnetized star.

Very recently, however, Muhlberger et al. (2014) performed accurate general relativistic magnetohydrodynamical simulations and found that the low-$T/|W|$ instability would be suppressed by a weaker magnetic field energy than given in Fu & Lai (2011b). In their simulation models, the large toroidal magnetic field ($\sim 10^{16}$G) is wound up from the initial poloidal field ($\sim 10^{14}$G) by differential rotation. Since the toroidal magnetic fields are wound up in their models, the distributions of the toroidal magnetic field are determined by the profile of the differential rotation. The distributions of the toroidal magnetic fields are different from the simple model used in Fu & Lai (2011b). The maximum strength of the local toroidal magnetic field reached approximately 10^{17} G in their simulations, but the total magnetic energy peaked at 0.56% of the kinetic energy T. Although this energy ratio ($\mathcal{M}/T \sim 5.6\times10^{-3}$) is much smaller than that in Fu & Lai (2011b) ($\mathcal{M}/T \sim 0.2$), the low-$T/|W|$ instability was stabilized by the toroidal magnetic fields in their simulation models. They also showed that slow magnetosonic resonances appear in their simulation models (fig. 10 in their paper). This result shows that both the total magnetic energy and the structure of the toroidal field are important for suppression by magnetic fields because low-$T/|W|$ instabilities significantly depend on the values of the local rotational velocity (degree of the differential rotation; Shibata et al. 2003). Fu & Lai (2011b), however, calculated only one simple toroidal magnetic field model which did not represent the wound magnetic field. Therefore, we must consider various toroidal magnetic fields in order to study the linear analysis and address the suppression systematically.

Although many equilibrium states with purely toroidal magnetic fields have been consistently obtained in both Newtonian (e.g., Miketinac 1973; Lander & Jones 2009; Fu & Lai 2011b) and general relativistic (e.g., Kiuchi & Yoshida 2008; Yasutake et al. 2010; Frieben & Rezzolla 2012; Pili et al. 2014) frameworks, all of their toroidal magnetic field configurations are essentially same-class solutions. When we calculate a stationary axisymmetric and barotropic rotating star with purely toroidal magnetic fields, we obtain two arbitrary functions from the integrability condition of the magnetohydrodynamic equation that are related to the rotation law of the angular velocity and the distribution of the toroidal magnetic field. Rotating equilibrium states have been studied and many rotation laws have been investigated in both Newtonian and general relativistic frameworks (e.g., Eriguchi & Mueller 1985; Hachisu 1986a; Komatsu et al. 1989a; Galeazzi et al. 2012). In contrast, only a few works have studied purely toroidal magnetized equilibrium states, Almost all previous works have employed only a simple functional form (Miketinac 1973; Kiuchi & Yoshida 2008; Lander & Jones 2009; Yasutake et al. 2010; Fu & Lai 2011b; Frieben & Rezzolla 2012; Pili et al. 2014). The functional form of a toroidal magnetic field is considered *rigid* in analogy to the rotation law. Although a *rigid* toroidal field is simple and widely accepted, the distributions of the toroidal field do not represent those wound up by differential rotation. Thus, we need to construct a *differential* toroidal magnetic field which represents magnetic winding by differential rotation and to treat the linear analysis and the suppression more systematically. As a first step, this paper investigate new functional forms of a *differential* field and obtains new solutions of purely toroidal magnetized equilibria. These solutions will be useful for equilibrium models for linear analysis.

The remainder of this paper is organized as follows. In Section 2, we describe the new functional forms of the arbitrary functions. In Section 3, we present results from numerical calculations. Discussion and conclusions are given in Section 4.

2 BASIC EQUATIONS AND FORMULATIONS

We employed the formulation developed by Kiuchi & Yoshida (2008) and Lander & Jones (2009). We will first briefly summarize the formulation below while the remainder of the section focuses on explaining the new functional forms in detail. Both cylindrical coordinates (ϖ, φ, z) and spherical coordinates (r, θ, φ) are utilized in this paper.

2.1 Assumptions and basic equations

As per previous works, we make the following assumptions for magnetized stars.

(i) The system is in a stationary state, i.e. $\partial/\partial t = 0$.
(ii) The rotational axis and magnetic axis coincide.
(iii) The configuration is axisymmetric about the rotational axis, i.e., $\partial/\partial\varphi = 0$.
(iv) There are no meridional flows or poloidal magnetic fields, i.e. the magnetic field is purely toroidal.
(v) The star is self-gravitating.
(vi) The system is treated in the framework of non-relativistic physics.
(vii) No electric current is assumed in the vacuum region.
(viii) There is no current sheet, i.e. the magnetic field continues smoothly.
(ix) The barotropic equation of state is assumed.

These assumptions are adopted here for simplicity. For a barotropic equation of state, we use a polytropic equation of state

$$P = K\rho^{1+1/N}, \tag{1}$$

where P and ρ are the gas pressure and the density, respectively, and K and N are constants.

Under these assumptions, the equations that describe this system are the Euler equations

$$\frac{1}{\rho}\nabla p = -\nabla\phi_g + \boldsymbol{F} + \boldsymbol{L}, \tag{2}$$

$$\boldsymbol{F} = \frac{v_\varphi^2}{\varpi}\,\boldsymbol{e}_\varpi + 0\,\boldsymbol{e}_\varphi + 0\,\boldsymbol{e}_z, \tag{3}$$

$$\boldsymbol{L} = \frac{1}{\rho}\left(\frac{\boldsymbol{j}}{c}\times\boldsymbol{B}\right) = \frac{1}{\rho}\left\{-\frac{j_z}{c}B_\varphi\boldsymbol{e}_\varpi + 0\,\boldsymbol{e}_\varphi + \frac{j_\varpi}{c}B_\varphi\boldsymbol{e}_z\right\}, \tag{4}$$

the integral form of the Poisson equation

$$\phi_g(\boldsymbol{r}) = -G\int\frac{\rho(\boldsymbol{r}')}{|\boldsymbol{r}-\boldsymbol{r}'|}\,dV' \tag{5}$$

and stationary Maxwell's equations,

$$\nabla\cdot\boldsymbol{B} = 0, \tag{6}$$

$$\nabla\times\boldsymbol{B} = 4\pi\frac{\boldsymbol{j}}{c}, \tag{7}$$

$$\nabla\times\boldsymbol{E} = 0, \tag{8}$$

where ϕ_g, v_φ, $\boldsymbol{j}$, c, B_φ, G and $\boldsymbol{E}$ are, respectively, the gravitational potential, the toroidal velocity, the current density, the speed of light, the toroidal magnetic field, the gravitational constant, and the electric field. Using these equations, we obtain the first integral of the Euler equation (see e.g., Lander & Jones 2009) as

$$\int\frac{dp}{\rho} = -\phi_g + \phi_R - \phi_M + C, \tag{9}$$

$$\phi_R = \int\Omega^2(\varpi)\varpi\,d\varpi, \tag{10}$$

$$\phi_M = \frac{1}{4\pi}\int\frac{I(\lambda)}{\lambda}\frac{dI(\lambda)}{d\lambda}\,d\lambda, \tag{11}$$

where C is an integral constant, and ϕ_R and ϕ_M are the rotational potential and the magnetic potential respectively. $\Omega(\varpi)$ and $I(\lambda)$ are arbitrary functions of ϖ and λ, respectively, and λ is a scalar function defined by $\lambda \equiv \rho\varpi^2$. These arbitrary functions are related to the toroidal velocity and the toroidal magnetic field according to

$$v_\varphi = \varpi\Omega(\varpi), \tag{12}$$

$$B_\varphi = \frac{I(\lambda)}{\varpi}. \tag{13}$$

Therefore, there appears to be two arbitrary functions when we calculate a rotating star with a purely toroidal magnetic field. Note that we can choose any kind of functional forms of these potentials respectively under the assumption of no poloidal magnetic field and no meridional flow, because the toroidal magnetic field does not produce a force that acts directly onto the rotation and the rotation does not change the toroidal magnetic field. We can obtain one rotating magnetized equilibrium solution by fixing these two functional forms. The arbitrary function Ω corresponds to the rotation law of the rotating star. We can obtain various differential rotating stars by changing the functional form of Ω. On the other hand, the physical meaning of the arbitrary function I is less clear. In all previous works, a simple functional form was adopted with no investigation of new functional forms that express various toroidal magnetic fields such as differential rotations. This paper discusses new functional forms of I that correspond to the toroidal magnetic field wound up by the differential rotation.

2.2 Functional forms of arbitrary functions and their physical meanings

First, we will review functional forms of Ω and discuss the rotation laws. The following three types of rotation law are usually used (see e.g., Eriguchi & Mueller 1985; Hachisu 1986a):

(i) rigid rotation:

$$\Omega^2(\varpi) = \Omega_0^2, \tag{14}$$

(ii) v-constant rotation:

$$\Omega^2(\varpi) = \frac{v_0^2}{(\varpi^2+d^2)}, \tag{15}$$

(iii) j-constant rotation:

$$\Omega^2(\varpi) = \frac{j_0^2}{(\varpi^2+d^2)^2}, \tag{16}$$

where Ω_0, v_0, j_0, and d are constants. d represents the degree of the differential rotation. As d increases for the latter two laws, their differential rotations approach rigid rotation. As d decreases towards zero, the latter two rotation laws approach the true rotation denoted by their respective names. That is, v_φ becomes strictly constant in space for the second law (v-constant rotation) and the specific angular momentum per unit mass, $j = \varpi^2\Omega$, becomes exactly constant in space for the third law (j-constant rotation). For these cases, we can obtain the explicit forms of the rotational potentials as follows.

(i) For rigid rotation:

$$\phi_R(\varpi) = \frac{\Omega_0^2\varpi^2}{2}, \tag{17}$$

(ii) For v-constant rotation:

$$\phi_R(\varpi) = \frac{v_0^2\ln(\varpi^2+d^2)}{2}, \tag{18}$$

(iii) For j-constant rotation:

$$\phi_R(\varpi) = -\frac{j_0^2}{2(\varpi^2+d^2)}. \tag{19}$$

These types of rotation laws have also been studied in general relativistic frameworks (e.g., Komatsu et al. 1989a,b). Recently, Galeazzi et al. (2012) studied rotation laws systematically and obtained a new functional form,

$$\Omega(\varpi) = \Omega_c\left\{1+\left(\frac{\varpi}{\varpi_0}\right)^2\right\}^{1/\gamma}, \tag{20}$$

where Ω_c and γ are constants. We can invoke a wide range of rotation laws by changing the value of γ (Galeazzi et al. 2012). Almost all works concerning the low-$T/|W|$ instability have applied the j-constant functional form for differential rotations of initial models (e.g., Shibata et al. 2002, 2003).

In contrast, only the following simple power-law type functional form of I has been adopted in previous works (Kiuchi & Yoshida 2008; Lander & Jones 2009; Yasutake et al. 2010; Frieben & Rezzolla 2012; Pili et al. 2014)

$$I(\lambda) = I_0\lambda^k, \tag{21}$$

where k is a constant. Since we have assumed that the magnetic field continues smoothly, the regularity of the toroidal magnetic field is required. The parameter k must be $k \geq 1$, because the functional form with $k \geq 1$ satisfies the regularity condition at the

centre ($B_\varphi \to 0$, $\varpi \to 0$). We can derive the magnetic potential using this power-law functional form as

$$\phi_M = \frac{I_0^2}{4\pi} k \int \lambda^{2k-2} d\lambda = \frac{I_0^2}{4\pi} \frac{k}{2k-1} \lambda^{2k-1} = \frac{I_0^2}{4\pi} \frac{k}{2k-1} (\rho\varpi^2)^{2k-1}. \quad (22)$$

As we have seen, the exponents of the rotational potential are $\phi_R \sim \varpi^2$ (rigid), $\phi_R \sim \varpi^{-1}$ (v-constant), and $\Phi_R \sim \varpi^{-2}$ (j-constant). The exponents of rotational potentials of the differential rotations are negative, while that of rigid rotation is positive. The exponent of the rotational potential characterize the rotation law. On the other hand, the magnetic potential becomes $\phi_M \sim \varpi^{4k-2} (k \geq 1)$ when the star is incompressible (Kiuchi & Yoshida 2008). Since k is limited to $k \geq 1$ by the boundary condition, the exponent of this magnetic potential is always positive. Therefore, we consider this functional form of magnetic potential as a *rigid* toroidal magnetic field in analogy to the rotation law.

If the toroidal magnetic field is wound up from the initial poloidal fields by the differential rotations, the distribution of the toroidal magnetic field is determined by the profile of this differential rotation. If we neglect the meridional flow, the evolution of the toroidal magnetic field is described by the following induction equation:

$$\frac{\partial B_\varphi}{\partial t} = \{\nabla \times (\boldsymbol{v} \times \boldsymbol{B})\}_\varphi \sim \frac{\partial}{\partial z}(v_\varphi B_z) + \frac{\partial}{\partial \varpi}(v_\varphi B_\varpi). \quad (23)$$

If the initial magnetic field is purely poloidal (B_p) and B_p only has a constant ϖ-component ($\boldsymbol{B}_p = B_0\, \boldsymbol{e}_\varpi + 0\, \boldsymbol{e}_\varphi + 0\, \boldsymbol{e}_z$), the poloidal field is wound up by the differential rotation and the profiles of the toroidal magnetic field become

$$B_\varphi \sim B_0 \frac{\partial}{\partial \varpi}(\varpi\Omega) \sim \begin{cases} \varpi^{-1} & (v-\text{const.}), \\ \varpi^{-2} & (j-\text{const.}). \end{cases} \quad (24)$$

Therefore, the toroidal magnetic field wound up by the differential rotation must satisfy the magnetic winding in equation (24), but we have not obtained such toroidal magnetic field distributions by using a *rigid* toroidal field (equation 21). Since the rotation and the toroidal magnetic field are not necessarily consistent with each other under the assumption of no meridional flow and no poloidal magnetic field, we can select the functional forms of $I(\lambda)$ that are most compatible with the chosen rotational potential.

Here, we introduce two new functional forms of I whose toroidal magnetic fields satisfy equation (24). We call the functional forms *differential* toroidal fields in analogy to rotation law and rotational potentials. The functional form of a type 1 *differential* toroidal field is

$$I(\lambda) = I_0 \frac{\lambda}{\sqrt{\lambda + h^2}} \quad (25)$$

and the functional form of a type 2 *differential* toroidal field is

$$I(\lambda) = I_0 \frac{\lambda}{\lambda + h^2}, \quad (26)$$

where h is a constant. h represents the degree of the *differential* toroidal magnetic field. The magnetic potentials of these functions are

$$\phi_M(\lambda) = \frac{I_0^2}{4\pi} \left\{ \frac{\ln(\lambda + h^2)}{2} - \frac{h^2}{2(\lambda + h^2)} \right\}, \quad (27)$$

for a type 1 *differential* magnetic potential and

$$\phi_M(\lambda) = -\frac{I_0^2}{4\pi} \frac{h^2}{2\,(\lambda + h^2)^2}, \quad (28)$$

for a type 2 *differential* magnetic potential. Since the exponents of these *differential* magnetic potentials are $\sim \varpi^{-2}$ in type 1 and $\sim \varpi^{-4}$ in type 2, we can obtain a wide range of the distributions of the toroidal magnetic field using these functional forms, including distributions which meet the condition of equation (24) (see the profiles of toroidal magnetic fields in fig. 1).

2.3 Numerical settings and accuracy check

Following previous works (Kiuchi & Yoshida 2008; Lander & Jones 2009), we adopted Hachisu's self-consistent scheme (Hachisu 1986a; Hachisu 1986b), which is a very powerful numerical scheme for obtaining a rotating star in equilibrium. In this scheme, we fix the axis ratio $q \equiv r_{pol.}/r_e$ to obtain the equilibrium configuration, where $r_{\rm pol.}$ and $r_{\rm e}$ are the polar radius and the equatorial radius, respectively. When we calculate magnetized rotating equilibria, we need to fix another parameter. We choose $\hat{I}_0$ in the arbitrary functions as the parameter in this paper. Thus, we fixed both q and $\hat{I}_0$ during our numerical iteration cycles and obtained one equilibrium state after the iteration.

The physical quantities are transformed to be dimensionless in actual numerical computations. We adopted the dimensionless forms in Fujisawa & Eriguchi (2013) by utlising the maximum density $\rho_{\rm max}$, the maximum pressure $p_{\rm max}$, and the equatorial radius r_e as follows:

$$\hat{r} \equiv \frac{r}{r_e} = \frac{r}{\sqrt{\frac{1}{\alpha}\frac{p_{\rm max}}{4\pi G \rho_{\rm max}^2}}}, \quad (29)$$

$$\hat{\rho} \equiv \frac{\rho}{\rho_{\rm max}}, \quad (30)$$

where α is introduced to ensure a unity distance from the centre to the equatorial surface of the star. Other physical quantities are also transformed to be dimensionless (see the Appendix in Fujisawa & Eriguchi 2013). A term with a hat () denotes a dimensionless quantity.

To see the global characteristics of magnetized rotating equilibria, we define some integrated quantities as follows:

$$W = \frac{1}{2} \int \rho \phi_g \, dV, \quad (31)$$

$$T = \frac{1}{2} \int \rho (\varpi\Omega)^2 \, dV, \quad (32)$$

$$\Pi = \int p \, dV, \quad (33)$$

$$U = N\Pi, \quad (34)$$

$$\mathcal{M} = \frac{1}{8\pi} \int B_\varphi^2 \, dV, \quad (35)$$

where W, T, Π, U, and $\mathcal{M}$ are the gravitational energy, the rotational energy, the total pressure, the internal energy, and the magnetic energy respectively. We also define the volume averaged magnetic field $B_{\rm ave}$ (Fujisawa et al. 2012) as

$$B_{\rm ave} \equiv \sqrt{\frac{\int B_\varphi^2 \, dV}{\int dV}} = \sqrt{\frac{8\pi\mathcal{M}}{V}}, \quad (36)$$

where V is the volume of the star. This term is useful when we

evaluate the localization of the magnetic field. We also calculate the toroidal Alfvén velocity as

$$V_A = \frac{B_\varphi}{\sqrt{4\pi\rho}}. \quad (37)$$

Note that we checked the numerical convergence by using the Virial theorem (Appendix A) and ensured a sufficient number of mesh points for numerical computations in this paper.

3 NUMERICAL RESULTS

This section shows our numerical solutions with differential rotation and a *differential* toroidal field. We fixed the polytropic index $N = 1$ as a simple equation of state for a proto-neutron star. We adopted the j-constant rotation law with $\hat{d} = 0.3$ as the differential rotation. The low-$T/|W|$ instability of this differential rotating star commences when the value of β becomes larger than 0.03 (Shibata et al. 2003). We fixed the axis ratio $q = 0.8$ and obtained the rotating equilibrium state whose β is 0.04. Panel (a) in fig. 2 is a density contour of this rotating star without toroidal magnetic fields. The isopycnic surfaces are distorted by the strong rotation. This rotating star gains the low-$T/|W|$ instability if it does not have a toroidal magnetic field.

To show the profiles of the re-dimensionalized toroidal magnetic fields, we used a neutron star's typical values of mass ($M = 1.4M_\odot$) and central density ($\rho_{\rm max} = 10^{15}{\rm g/cm^3}$). The maximum strength of the magnetic field is approximately a few times 10^{16} G and the maximum value of the Alfvén velocity is a few times $10^8{\rm cm/s}$ in this model.

3.1 *Differential* toroidal magnetic field

First, we will compare one non-magnetized equilibrium state and six magnetized equilibrium states with *rigid* or *differential* toroidal fields. The numerical models and results are tabulated in table 1 and plotted in figures 1 and 2. The relative value of the Virial relation (VC) in all solutions is very small (see accuracy verification in Appendix A). We calculated many magnetized equilibrium states and displayed some solutions whose ratios of the rotational energy to magnetic energy are equal ($\mathcal{M}/T = 1.0 \times 10^{-2}$). This energy ratio is smaller than Fu & Lai's criterion ($\mathcal{M}/T \sim 2.0\times10^{-1}$), but larger than that of Muhlberger et al. (2014) ($\mathcal{M}/T \sim 5.6 \times 10^{-3}$). These toroidal magnetic fields could suppress the low-$T/|W|$ instability.

Since the values of β for these solutions are almost the same, their magnetic energies are also almost the same. As seen in Table 1, however, the ratio $B_{\rm max}/B_{\rm ave}$ is different for each model. The ratio for the *rigid* toroidal solution with $k = 1$ is 1.88. This value is almost as the same as those for the type 1 *differential* toroidal solution with $\hat{h} = 0.1$ (1.70) or the type 2 *differential* toroidal solutions with $\hat{h} = 0.1$ (1.8) and $\hat{h} = 0.2$ (1.99). On the other hand, the ratios of the *rigid* toroidal solution with $k = 2$ and the type 2 *differential* toroidal solution with $\hat{h} = 0.3$ are 2.48 and 2.77, respectively. These larger values indicate that the toroidal fields of these two models are more localized than those of other solutions.

The profiles of the toroidal magnetic fields are different and rely heavily on their type. Fig. 1 displays the profiles of $d\hat{\varpi}\hat{\Omega}/d\hat{\varpi}$ (left-hand panel) and the re-dimensionalized B_φ (right-hand panel). The curves represent the following: (i) the thick solid curve shows a type 2 *differential* field with $\hat{h} = 0.1$, (ii) the thick dashed curve shows a type 2 *differential* field with $\hat{h} = 0.2$, (iii) the thick dotted curve shows a type 1 *differential* field with $\hat{h} = 0.1$, (iv) the thin solid curve shows a *rigid* field with $k = 1$ and (v) the thin dashed curve shows a *rigid* field with $k = 2$. The magnetic winding by the differential rotation ($d\hat{\varpi}\hat{\Omega}/\hat{\varpi}$ in the left-hand panel) reaches a maximum value at the rotational axis $\hat{\varpi} = 0$ and the value decreases rapidly near the centre. On the other hand, the profiles of the *rigid* toroidal fields reach maximum values in the middle regions [$\hat{\varpi} \sim 0.5$ with $k = 0$ (curve iv) and $\hat{\varpi} \sim 0.6$ with $k = 1$ (curve v)]. These distributions do not represent the magnetic winding by the differential rotation ($d\hat{\varpi}\hat{\Omega}/d\hat{\varpi}$ in the left-hand panel). The profile of the type 1 *differential* toroidal field is gradual. The ratio of $B_{\rm max}/B_{\rm av.}$ is the smallest among these seven solutions. This functional form of I corresponds to B_φ-constant toroidal fields such as the v-constant rotation law, because the functional form of the type 1 *toroidal* field is $I \sim \varpi(B_\varphi = {\rm const.})$ when the star is incompressible.

In contrast, the value of the type 2 *differential* toroidal fields reach a maximum near the rotational axis [$\hat{\varpi} \sim 0.2$ with $\hat{h} = 0.2$ (curve ii) and $\hat{\varpi} \sim 0.1$ with $\hat{h} = 0.1$ (curve i)]. As the value of $\hat{h}$ decreases, the degree of the *differential* toroidal field becomes large and the maximum point reaches the rotational axis. These type 2 *differential* toroidal fields resemble the magnetic winding by the differential rotation. In particular, the toroidal field with $\hat{h} = 0.1$ closely matches the magnetic winding (fig. 1). Therefore, we can obtain the toroidal field wound up by differential rotation by using type 2 *differential* toroidal fields under the assumption that initial profile of the magnetic field is uniform (equation 24) .

Fig. 2 shows the contour maps of $\hat{\rho}$ and $\hat{B}_\varphi$ for these solutions. Panel (a) displays the density distribution of the non-magnetized solution. Since the magnetic energy of our solutions is smaller than the gravitational energy ($\mathcal{M}/|W| = \mathcal{M}/T \times T/|W| \sim 10^{-4}$), all solutions in table 1 have similar isopycnic surfaces. The other panels show distributions of the toroidal fields. Panel (b) shows the contour of a *rigid* toroidal field with $k = 1$. This configuration is the same as those in previous works (e.g., see fig. 2 in Lander & Jones 2009). Panels (c) and (d) display a type 1 *differential* field with $\hat{h} = 0.1$ and a type 2 *differential* field with $\hat{h} = 0.1$, respectively. As we see in fig. 1, the toroidal magnetic fields of a type 2 *differential* field are concentrated and localized near the rotational axis.

3.2 Highly localized *differential* toroidal magnetic field

Next, we calculated the type 2 *differential* toroidal field by changing the value of $\hat{h}$ and compared the resulting models and the *rigid* toroidal field model. We show one *rigid* toroidal model and six *differential* toroidal models. Since $\hat{h}$ determines the degree of the *differential* toroidal magnetic field, the toroidal magnetic field is localized and concentrated near the centre when the value decreases. We calculated many equilibrium states by changing the value of $\hat{h}$ and $\hat{I}_0$, and obtained one solution sequence. The numerical results of the solution sequence are tabulated in Table 2 and the profiles of the re-dimensionalized toroidal magnetic fields and the Alfvén velocity are plotted in fig. 3. In this sequence, the local maximum values of the *differential* toroidal magnetic fields are comparable to those of a *rigid* field at that point (see fig. 3).

As seen in fig. 3, the location of the maximum point approaches the centre as the value of $\hat{h}$ decreases. This is because the degree of the *differential* toroidal magnetic field increases. The maximum point of the *rigid* toroidal field is located at $\hat{\varpi} \sim 0.5$ and that point in the *differential* toroidal fields becomes $\hat{\varpi} \sim 0.4$ ($\hat{h} = 0.5$), $\hat{\varpi} \sim 0.2$ ($\hat{h} = 0.2$), $\hat{\varpi} \sim 0.1$ ($\hat{h} = 0.1$) and

Table 1. Numerical results for each model. All solutions have almost the same magnetic energy.

q	$\hat{I}_0^2$	k or $\hat{h}$	β	$\mathcal{M}/T$	$B_{\max}(G)$	$B_{\max}/B_{\rm ave}$	$V_{A\,\max}$ (cm/s)	VC
No magnetic								
0.8	0	-	4.00E-2	0.00E0	0	-	-	1.11E-5
Rigid toroidal								
0.8	7.12E-3	$k=1$	4.02E-2	1.00E-2	3.67E16	1.88	4.14E8	1.12E-5
0.8	2.95E-1	$k=2$	4.02E-2	1.00E-2	4.84E16	2.48	5.78E8	1.12E-5
Type 1 *differential* toroidal								
0.8	9.27E-4	$\hat{h}=0.1$	4.02E-2	1.00E-2	3.30E16	1.70	3.15E8	1.12E-5
Type 2 *differential* toroidal								
0.8	3.32E-4	$\hat{h}=0.3$	4.02E-2	1.00E-2	3.50E16	1.80	3.20E8	1.12E-5
0.8	1.72E-4	$\hat{h}=0.2$	4.02E-2	1.00E-2	3.85E16	1.99	3.45E8	1.12E-5
0.8	8.30E-5	$\hat{h}=0.1$	4.03E-2	1.00E-2	5.39E16	2.77	4.80E8	1.15E-5

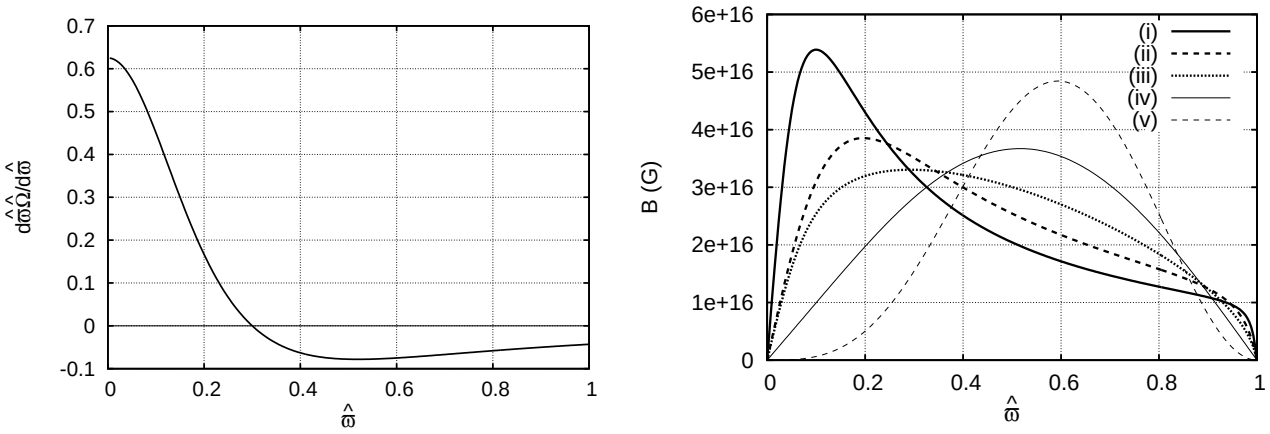

Figure 1. Left: the profile of $d\hat{\varpi}\hat{\Omega}/d\hat{\varpi}$ with $\hat{d}=0.3$ j-constant rotation. Right: the profiles of B_φ on the equatorial plain. The vertical axis denotes the re-dimensionalized toroidal magnetic field in units of Gauss. (i) Type 2 differential toroidal field with $\hat{h}=0.1$. (ii) Type 2 differential toroidal field with $\hat{h}=0.2$. (iii) Type 1 differential toroidal field with $\hat{h}=0.1$. (iv) Rigid toroidal field with $k=1$. (v) Rigid toroidal field with $k=2$.

Table 2. Numerical results for each model.

q	$\hat{I}_0^2$	$\hat{h}$	β	$\mathcal{M}/T$	$B_{\max}$ (G)	$B_{\max}/B_{\rm ave}$	$V_{A\,\max}$ (cm/s)	VC
Rigid toroidal								
0.8	7.12E-3	-	4.02E-2	1.00E-2	3.67E16	1.88	4.14E8	1.12E-5
Type 2 *differential* toroidal								
0.8	1.00E-3	0.5	4.02E-2	9.44E-3	3.31E16	1.75	3.32E8	1.12E-5
0.8	5.00E-4	0.4	4.02E-2	8.25E-3	3.09E16	1.75	2.94E8	1.12E-5
0.8	2.00E-4	0.3	4.01E-2	6.05E-3	2.71E16	1.79	2.48E8	1.12E-5
0.8	5.00E-5	0.2	4.01E-2	2.91E-3	2.08E16	1.98	1.86E8	1.12E-5
0.8	3.50E-6	0.1	4.01E-2	4.21E-4	1.10E16	2.76	9.84E7	1.12E-5
0.8	1.50E-7	0.05	4.00E-2	2.83E-5	4.56E15	4.41	4.07E7	1.11E-5

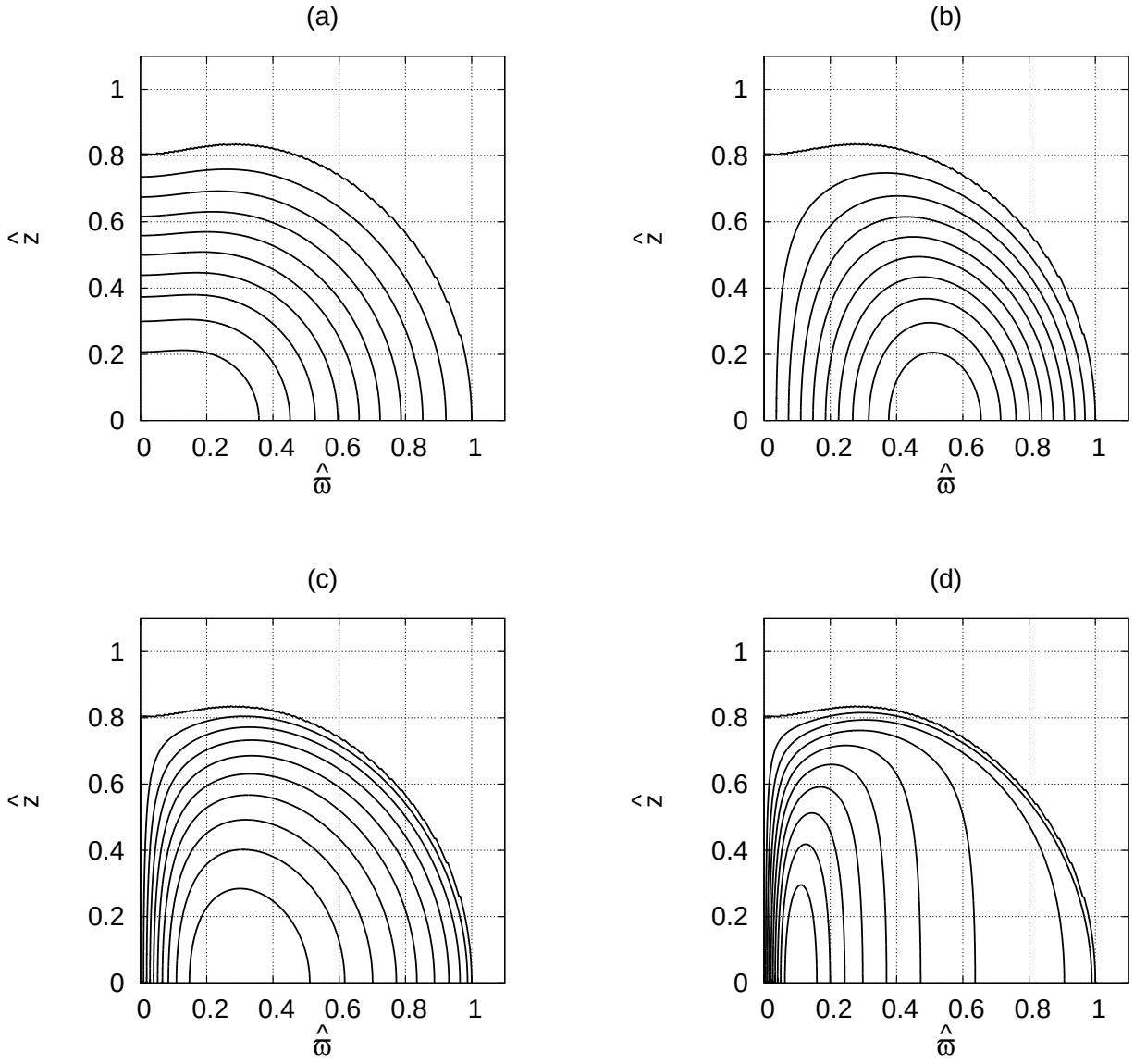

Figure 2. Contours of $\hat{\rho}$ and the toroidal magnetic field ($\hat{B}_\varphi$). The difference between the two adjacent contours is 1/10 of the maximum value of $\hat{\rho}$ or $\hat{B}_\varphi$. (a) The contour of a ρ with non-magnetic field. (b) The contour of a $\hat{B}_\varphi$ of rigid toroidal field with $k = 1$. (c) The contour of a $\hat{B}_\varphi$ of type 1 differential toroidal field with $\hat{h} = 0.1$. (d) The contour of a $\hat{B}_\varphi$ of type 2 differential toroidal field with $\hat{h} = 0.1$.

$\hat{\varpi} \sim 0.05$ ($\hat{h} = 0.05$) as seen in the left-hand panel of fig. 3. The profiles of Alfvén velocities have the same tendency in the right-hand panel. The values of the ratio $B_{\max}/B_{\rm ave}$ increases as the degree of the *differential* increases. The ratios are $1.75(\hat{h} = 0.5)$, $1,98(\hat{h} = 0.2)$, $2.76(\hat{h} = 0.1)$ and (4.41 $\hat{h} = 0.05$). Thus, the *differential* toroidal magnetic field is localized and concentrated near the centre when the degree of the *differential* is large.

However, the magnetic field energy ratios ($\mathcal{M}/T$) of the *differential* toroidal field solutions are much smaller than that of the *rigid* one (Table 2). As fig. 3 shows, the strength of the magnetic field and the Alfvén velocity in each differential model near the local maximum point are almost the same as those of the *rigid* model at the same radius. However, the magnetic energies of the differential models are smaller than that of the *rigid* model because of their localization and concentration near the point. Although the magnetic energy ratio ($\mathcal{M}/T$) of the *rigid* solution is $\sim 1.0 \times 10^{-2}$, the energy ratios of type 2 *differential* solutions with small $\hat{h}$ are $\sim 2.91 \times 10^{-3}$ ($\hat{h} = 0.2$), $\sim 4.21 \times 10^{-4}$ ($\hat{h} = 0.1$), and $\sim 2.85 \times 10^{-5}$ ($\hat{h} = 0.05$). The magnetic energy of the type 2 *differential* toroidal solution with $\hat{h} = 0.05$ is much smaller than that of the *rigid* toroidal model, even if the strength of the toroidal magnetic field is comparable to that of the *rigid field* at the local maximum point ($\hat{\varpi} \sim 0.05$). The localisation and concentration of the toroidal magnetic field near the rotational axis can be realized by using type 2 *differential* toroidal fields.

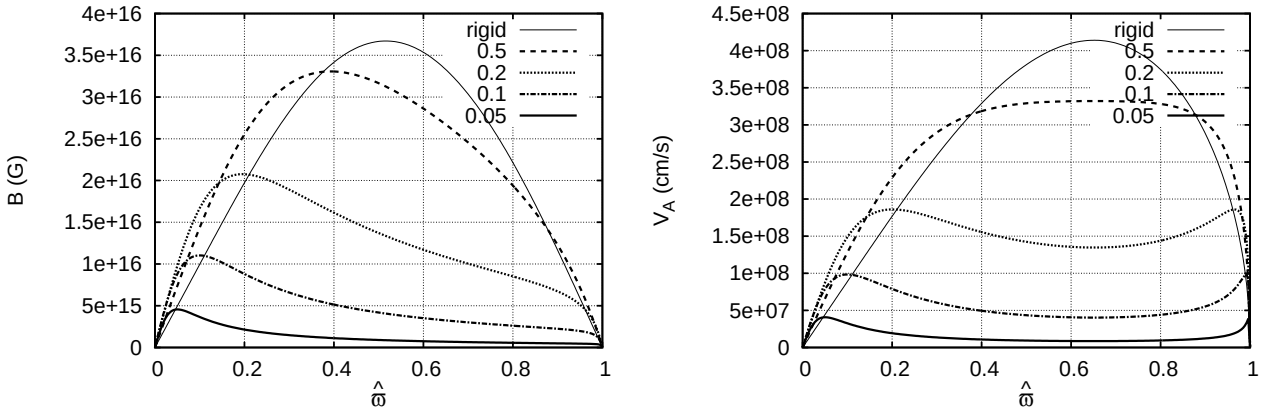

Figure 3. Left: the profiles of B_φ on the equatorial plane. Each curve denotes a rigid field with $k = 1$ (thin solid), and a type 2 differential field with $\hat{h} = 0.5$ (thick dashed), $\hat{h} = 0.2$ (thick dotted), $\hat{h} = 0.1$ (thick dot-dashed) and $\hat{h} = 0.05$ (thick solid). Right: the profiles of V_A on the equatorial plane. Each curve denotes a *rigid* field with $k = 1$ (thin solid), and a type 2 *differential* field with $\hat{h} = 0.5$ (thick dashed), $\hat{h} = 0.2$ (thick dotted), $\hat{h} = 0.1$ (thick dot-dashed) and $\hat{h} = 0.05$ (thick solid).

4 DISCUSSION AND CONCLUDING REMARKS

4.1 Suppression of the low-$T/|W|$ instability by low $\mathcal{M}/T$ magnetic fields

The low-$T/|W|$ instability is related to the corotation point inside the star (Andersson 2003). Since the wave pattern speed of an unsTable mode is equal to the rotational velocity of the background star, the corotation resonance would be driven at the point. Recent time evolutions of linear analysis have shown that the f mode becomes unsTable when the corotation point appears inside the star (Passamonti & Andersson 2015). The low-$T/|W|$ instability depends on the degree of the differential rotation (Shibata et al. 2003), but the location of the corotation point is not obvious. Linear analysis has also illustrated that the location of the corotation point depends on both the degree of the differential rotation and the value of β (Passamonti & Andersson 2015). As the value of β decreases and the degree of the differential rotation increases, the location approaches the rotational axis. If the value of β is 0.04 and the degree of the differential rotation is $\hat{d} = 0.3$ as we have calculated in this paper, the corotation point will appear at $\hat{\varpi} \sim 0.27$ (see fig. 6 in Passamonti & Andersson 2015). Therefore, the location of the corotation point will appear near the rotation axis in a differential rotating star.

The suppression of the toroidal magnetic field may depend on the local strength of the toroidal magnetic field and Alfvén velocity, since the slow-magnetosonic points are determined locally by the values of density and toroidal magnetic fields at the point (Fu & Lai 2011b). As seen in figures 1 and 3, the maximum point of the *rigid* toroidal magnetic field is located at $\hat{\varpi} \sim 0.5$ – 0.6. These values are larger than the location of the corotation point ($\hat{\varpi} \sim 0.27$). On the other hand, the maximum point of the type 2 *differential* toroidal magnetic field is located at the inner region of the star. The maximum point is located at $\hat{\varpi} \sim 0.2$ when the degree of the *differential* is $\hat{h} = 0.2$. The location approaches the rotation axis as the degree of the *differential* toroidal magnetic field increases (fig. 3). Since the *differential* toroidal magnetic field represents the magnetic winding by the differential rotation very well (fig. 1), the profile of the toroidal magnetic field would become that of the type 2 *differential* toroidal magnetic fields if the toroidal field is wound up from the initial poloidal magnetic field by the differential rotation. If the star has a large differential rotation, the degree of the *differential* toroidal magnetic field would also become large because the toroidal field is developed by the magnetic winding. As a result, both the maximum point of the toroidal magnetic field and the corotation point approach the rotational axis. We assume that both points appear near the centre when the star has a large differential rotation. Such a *differential* toroidal field would suppress the low $T/|W|$ instability easily, even if the total magnetic field energy ratio ($\mathcal{M}/T$) were much smaller than that of the *rigid* toroidal field, because the strength of the local toroidal magnetic field and Alfvén velocity are comparable to those of the *rigid* toroidal field (fig. 3).

Such low-$\mathcal{M}/T$ suppression might be realized by the type 2 *differential* toroidal field. Since Muhlberger et al. (2014) calculated both rotation and magnetic winding simultaneously, the distribution of their toroidal magnetic field would be type 2 *differential* rather than *rigid*. The suppression of the low-$T/|W|$ instability might occur in a *differential* magnetic field configuration even if the magnetic energy ratio is very small. On the other hand, Fu & Lai (2011b) adopted a simple *rigid* toroidal magnetic field solution as a background model for their linear analysis. The suppression of the low-$T/|W|$ instability might need larger toroidal magnetic field energy than is available from a *differential* field because the maximum point of the toroidal field is located at the outer region of the corotation point.

The suppression would depend on the degree of the *differential* toroidal field as the low-$T/|W|$ instability depends on the degree of the differential rotation. In order to study the low-$\mathcal{M}/T$ suppression systematically, in the future, we will perform linear analysis using the *differential* toroidal field obtained here. Such work may explain the difference in the energy ratio ($\mathcal{M}/T$) between a linear analysis with a *rigid* toroidal field (Fu & Lai 2011b) and a numerical simulation with a *differential* toroidal field made by magnetic winding (Muhlberger et al. 2014).

4.2 Concluding remarks

We investigated new magnetized equilibria with differential rotation and *differential* toroidal fields in this paper. We developed new functional forms for *differential* toroidal fields in analogy to the rotation law of the differential rotation and obtained equilib-

rium states self-consistently by using a self-consistent numerical scheme.

The *differential* toroidal magnetic fields have two functional forms. The functional form of the type 1 *differential* toroidal field is similar to the v-constant differential rotation law. The profile of the toroidal field is a gradual slope (fig. 1). Since the toroidal magnetic field becomes constant when the star is incompressible, the type 1 *differential* toroidal magnetic field is analogous to a B_φ-constant toroidal field law. The type 2 *differential* toroidal field is similar to the j-constant rotational law. Such *differential* toroidal fields represent the magnetic winding by the j-constant differential rotation very well. The profiles of the toroidal magnetic fields represent the magnetic winding by the differential rotation (fig. 1). The type 2 *differential* toroidal field is localized and concentrated near the rotational axis when the degree of the *differential* toroidal magnetic field is large (fig. 2).

The low-$T/|W|$ instability would be suppressed by the concentrated and localized *differential* toroidal fields more efficiently than a *rigid* toroidal field. The maximum strength of the *differential* toroidal magnetic field can be locally comparable to that of a *rigid* toroidal magnetic field, even if the total magnetic energy of the *differential* field is much smaller than that of a *rigid* one (fig. 3). Since the low-$T/|W|$ instability and the suppression by the toroidal magnetic field would depend on the strength of the local rotational velocity and the toroidal magnetic field, the localized and concentrated *toroidal* magnetic field is efficient for the suppression even if the total magnetic energy is small. Such low-$\mathcal{M}/T$ suppression would be realized by the *differential* toroidal field wound up from the initial poloidal magnetic field by differential rotation. The *differential* toroidal magnetic field plays a key role in explaining the difference in the energy ratio ($\mathcal{M}/T$) between a linear analysis with a *rigid* toroidal field (Fu & Lai 2011b) and a numerical simulation with a *differential* toroidal field wound up from the initial poloidal magnetic field by differential rotation (Muhlberger et al. 2014).

ACKNOWLEDGEMENTS

The author would like to thank the anonymous reviewer for useful comments. K.F. would like to thank the members of the GG seminar and H. Okawa for valuable and useful comments. K.F. is supported by Grant-in-Aid for Scientific Research on Innovative Areas, no. 24103006.

REFERENCES

Akiyama S., Wheeler J. C., Meier D. L., Lichtenstadt I., 2003, ApJ, 584, 954
Andersson N., 2003, Classic. Quantum Gravity, 20, 105
Bryan G. H., 1889, Phil. Trans. R. Soc. A, 180, 187
Camarda K. D., Anninos P., Fragile P. C., Font J. A., 2009, ApJ, 707, 1610
Centrella J. M., New K. C. B., Lowe L. L., Brown J. D., 2001, ApJ, 550, L193
Chandrasekhar S., 1969, Ellipsoidal Figures of Equilibrium. Yale Univ. Press, New Haven, CT
Eriguchi Y., Mueller E., 1985, A&A, 146, 260
Franci L., De Pietri R., Dionysopoulou K., Rezzolla L., 2013, Phys. Rev. D, 88, 104028
Frieben J., Rezzolla L., 2012, MNRAS, 427, 3406
Fu W., Lai D., 2011a, MNRAS, 410, 1617
—, 2011b, MNRAS, 413, 2207
Fujisawa K., Eriguchi Y., 2013, MNRAS, 432, 1245
Fujisawa K., Yoshida S., Eriguchi Y., 2012, MNRAS, 422, 434
Galeazzi F., Yoshida S., Eriguchi Y., 2012, A&A, 541, A156
Hachisu I., 1986a, ApJS, 61, 479
—, 1986b, ApJS, 62, 461
Karino S., Eriguchi Y., 2003, ApJ, 592, 1119
Kiuchi K., Yoshida S., 2008, Phys. Rev. D, 78, 044045
Komatsu H., Eriguchi Y., Hachisu I., 1989a, MNRAS, 237, 355
—, 1989b, MNRAS, 239, 153
Lai D., Shapiro S. L., 1995, ApJ, 442, 259
Lander S. K., Jones D. I., 2009, MNRAS, 395, 2162
Masada Y., Takiwaki T., Kotake K., Sano T., 2012, ApJ, 759, 110
Miketinac M. J., 1973, Ap&SS, 22, 413
Muhlberger C. D., Nouri F. H., Duez M. D., Foucart F., Kidder L. E., Ott C. D., Scheel M. A., Szilágyi B., Teukolsky S. A., 2014, Phys. Rev. D, 90, 104014
Obergaulinger M., Aloy M. A., Müller E., 2006, A&A, 450, 1107
Obergaulinger M., Cerdá-Durán P., Müller E., Aloy M. A., 2009, A&A, 498, 241
Ostriker J., 1965, ApJS, 11, 167
Ott C. D., Dimmelmeier H., Marek A., Janka H.-T., Hawke I., Zink B., Schnetter E., 2007, Physical Review Letters, 98, 261101
Ott C. D., Ou S., Tohline J. E., Burrows A., 2005, ApJ, 625, L119
Papaloizou J. C. B., Pringle J. E., 1984, MNRAS, 208, 721
Passamonti A., Andersson N., 2015, MNRAS, 446, 555
Pili A. G., Bucciantini N., Del Zanna L., 2014, MNRAS, 439, 3541
Saijo M., Baumgarte T. W., Shapiro S. L., 2003, ApJ, 595, 352
Saijo M., Yoshida S., 2006, MNRAS, 368, 1429
Sawai H., Yamada S., Suzuki H., 2013, ApJ, 770, L19
Shibata M., Karino S., 2004, Phys. Rev. D, 70, 084022
Shibata M., Karino S., Eriguchi Y., 2002, MNRAS, 334, L27
—, 2003, MNRAS, 343, 619
Shibata M., Liu Y. T., Shapiro S. L., Stephens B. C., 2006, Phys. Rev. D, 74, 104026
Shibata M., Sekiguchi Y.-I., 2005, Phys. Rev. D, 71, 024014
Shu F. H., 1992, Physics of Astrophysics, Vol. II. University Science Books, Mill Valley, CA
Tomimura Y., Eriguchi Y., 2005, MNRAS, 359, 1117
Watts A. L., Andersson N., Jones D. I., 2005, ApJ, 618, L37
Yasutake N., Kiuchi K., Kotake K., 2010, MNRAS, 401, 2101

APPENDIX A: ACCURACY VERIFICATION

To check the numerical accuracy, we computed a relative value of the Virial relation as follows:

$$\mathrm{VC} \equiv \frac{|2T + W + 3\Pi + \mathcal{M}|}{|W|}. \tag{A1}$$

Our numerical domain is defined as $0 \leq \hat{r} \leq 1$ in the radial direction and $0 \leq \theta \leq \pi/2$ in the angular direction. Fig. A1 displays the value of VC as a function of the number of grid points in the r-direction. To plot this graph, we computed the solutions with j-constant differential rotation and a type 2 *differential* toroidal field ($\hat{h}$ = 0.3) changing the number of grid points in the r-coordinate, but fixing the number of grid points in the θ-direction as $n_\theta = 513$ (Fujisawa et al. 2012). The value of VC decreases in proportion to the square inverse of the number of grid points (Lander & Jones 2009; Fujisawa et al. 2012), because we

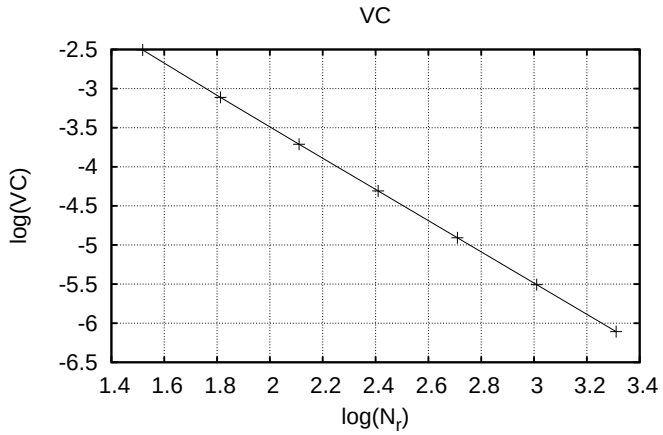

Figure A1. The Virial quantity VC, plotted against the number of grid points in the r-direction.

adopted Simpson's scheme as an integral method in our numerical code. The typical value of VC is smaller than $10^{-4} - 10^{-5}$ when the mesh numbers were $N_r = 513$ and $N_\theta = 513$. This value is sufficiently small and the system converges very well (cf. Hachisu 1986a; Tomimura & Eriguchi 2005; Lander & Jones 2009; Fujisawa & Eriguchi 2013). Thus, we fixed $N_r = 513$ and $N_\theta = 513$ in all calculations in this paper.